Thermal decomposition of allantoin as probed by matrix isolation FTIR spectroscopy

N. Kuş [a,b], S. Haman Bayarı [c], R. Fausto [b,*]

[a] Department of Physics, Anadolu University, 26470 Eskişehir, Turkey
[b] Department of Chemistry, University of Coimbra, P-3004-535 Coimbra, Portugal
[c] Hacettepe University, Faculty of Education, Department of Physics, 06800 Beytepe, Ankara, Turkey

ABSTRACT

The optimized geometries, energies of the possible conformers of allantoin (2,5-dioxo-4-imidazolidinyl urea, the diureide of glyoxylic acid) as well as the barriers for conformational interconversion have been calculated using the density functional theory [DFT(B3LYP)/6-311++G(d,p)] method. The calculations predicted the existence of four conformers (**gC**, **tT**, **g′C**, and **g′T**; where the first and second symbols in the name of the conformers designate the conformation around the exocyclic NHC–NHCO and CNH–CO axes, respectively), with the **gC** form contributing to more than 98% of the population in gas phase at room temperature. This conformer is different from that corresponding to the monomeric unit found in crystalline *RS*-allantoin (**g′C**; Mootz, D. *Acta Crystallogr.* **1965**, *19*, 726), stressing the importance of intermolecular H-bonding in determining the structure of the crystal. Upon sublimation under vacuum (10^{-6} mbar), the compound was found to undergo extensive decomposition to urea, isocyanic acid, NH_3, and carbon. The identification of the decomposition products was made by using matrix isolation in-frared spectroscopy. In consonance with the theoretical predictions, the allantoin molecules surviving thermal decomposition were found to undergo conformational isomerization and be present in the cryogenic argon matrix in both the **gC** and **g′C** conformations. The solid state room temperature infrared spectrum of allantoin was also investigated and assigned.

© 2009 Elsevier Ltd. All rights reserved.

1. Introduction

Allantoin (2,5-dioxo-4-imidazolidinyl urea; $C_4H_6N_4O_3$; Fig. 1) is also called 5-ureidohydantoin or glyoxyldiureide and is the diureide of glyoxylic acid. It is a product of purine metabolism and known
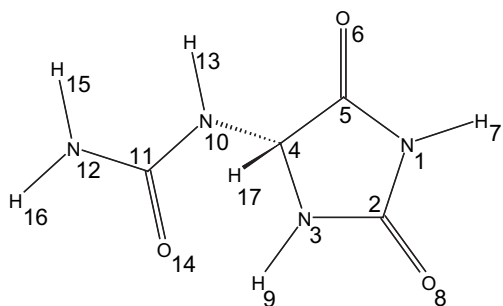

Figure 1. Allantoin, with the adopted atom labeling scheme.

* Corresponding author. Tel.: +351 239 852080; fax: +351 239 827703.
   E-mail address: rfausto@ci.uc.pt (R. Fausto).

since long ago to exist in nature, for example, in allantoic and am-niotic fluids, in fetal urine and in many plants and bacteria.[1–8] Al-lantoin is active in skin-softening and rapid skin cells regeneration. It removes corneocytes by loosening the intercellular kit or the desmosomes (protein bridges) that maintain the adhesion of cor-neocytes to each other. It then exfoliates dry and damaged cells and boosts the radiant appearance of the skin, whose surface becomes smoother and softer. Due to these properties, allantoin has been used in cosmetic industry in several forms (e.g., lotions, creams, suntan products, shampoos, lipsticks, and various aerosol prepara-tions), as well as in topical pharmaceutical preparations for treat-ment of skin diseases for many years.[4,9–11]

From a more fundamental perspective, allantoin is also an in-teresting compound, in which different types of intra- and in-termolecular H-bond interactions can be expected to be relevant in determining its structural preferences, spectroscopic properties, and reactivity. In particular, the fragmentation reactions exhibited by the compound appeared to us particularly appealing for investigation since the structure of the allantoin ring, with two sequential –C(=O)–N(H)– fragments, looked a good candidate to act as a precursor of isocyanic acid, a well known biologically pernicious substance that can easily react with amino terminus residues of proteins (or side chains of lysine and arginine residues) to form carbamoylated

proteins, which have been observed in several states of disease.[12–15] Indeed, 1-phenyl-tetrazolone, which has structural similarities to allantoin possessing a single –C(=O)–N(H)– fragment in its heterocyclic ring has been recently shown to decompose easily to phenylazide and isocyanic acid.[16]

In spite of both its many applications and expected interesting molecular properties and reactivity, allantoin has not yet been much studied from the structural point of view, though many publications describe procedures for its analytical determination, in particular in a biochemical context.[17–20] The molecule has a chiral center and may then exist as R- and S-enantiomeric forms. Contrary to what happens for the enantiomerically pure substance, for which no crystal data has yet been reported, the crystalline structure of RS-allantoin was obtained by X-ray diffraction.[21] The crystal was found to belong to the $P2_1/c$ space group (a=8.024, b=5.153, c=14.797 Å, β=93.01°), with four molecules in the unit cell, exhibiting an intricate three-dimensional H-bond network in which the three carbonyl oxygens, three imido, and two amino hydrogen atoms take part. The monomeric unit in the crystal was found to have the C_4–N_{10}–C_{11}–O_{14} axis in the cis conformation and a conformation around the C_4–N_{10} bond that directs the O_{14} atom to above the heterocyclic ring, so that the molecule assumes a 'scorpion like' geometry.[21]

Kahn and Tipton[22] performed simple HF/6-31G(d,p) calculations on the isolated molecule of allantoin and reported the existence of four different conformers, with the form similar to the monomeric structure found in the RS-allantoin crystal being the second most stable one. According to the HF/6-31G(d,p) calculations, the most stable conformer (by 12.8 kJ mol^{-1}) has also a cis C_4–N_{10}–C_{11}–O_{14} axis, but in this case the ureido group is directed toward the outside part of the molecule. Two additional conformers of higher energy bearing a trans C_4–N_{10}–C_{11}–O_{14} fragment were also described by Kahn and Tipton.[22] NMR data[22] showed that in solution of both DMSO or CHCl$_3$ allantoin should exist in a conformation with a cis C_4–N_{10}–C_{11}–O_{14} axis as well, though no precise identification of the relevant form could be undertaken.

Previously reported reactivity studies on allantoin have focused mainly on its racemization reaction.[22,23] To the best of our knowledge, no further structural or spectroscopic studies were reported on allantoin hitherto.

In the present investigation, we performed a detailed study of the potential energy surface of allantoin using the density functional theory (DFT) approach and investigated the thermal fragmentation of the compound taking place upon sublimation. The identification of the decomposition products was made by using matrix isolation infrared spectroscopy. In addition, we obtained and assigned the room temperature infrared spectrum of the compound. This enabled us to obtain further information on the most relevant intermolecular interactions that stabilize the **g′C** conformer in this phase over the thermodynamically most stable **gC** conformer.

2. Experimental and computational methods

Allantoin was provided by Prof. Mustafa Korkmaz, Hacettepe University, Ankara, spectroscopic grade (>98 %). The matrices were prepared by co-deposition of argon (99.99990% purity, obtained from Air Liquide) and the vapors generated upon sublimation of allantoin onto the cooled (10 K) CsI substrate of the cryostat (APD Cryogenics close-cycle helium refrigeration system with a DE-202A expander). A glass vacuum system and standard manometric procedures were used to deposit the isolating gas. Allantoin was placed in a specially designed mini-oven assembled inside the cryostat and thermoelectrically heated.

The matrix isolation IR spectra were collected, with 0.5 cm^{-1} spectral resolution, on a Nicolet 6700 Fourier Transform infrared

spectrometer, equipped with a deuterated triglycine sulfate (DTGS) detector and a Ge/KBr beamsplitter. The infrared spectrum of the neat RS-allantoin crystal in KBr pellet at room temperature was obtained in a BOMEM MB104 FTIR spectrometer, with resolution 4 cm^{-1}.

Differential Scanning Calorimetry (DSC) measurements were made in a Perkin–Elmer DSC7 calorimeter over the temperature range 25–255 °C, with scanning rate 10 °C min^{-1}. Data acquisition and determination of the onset temperatures were performed with the Perkin–Elmer 1020 Series Thermal Analysis System Software. The samples were hermetically sealed in aluminum pans, and an empty pan was used as reference. A 20 mL min^{-1} nitrogen purge was employed. Temperature calibration [24] was performed with high grade standards, namely biphenyl (T_{fus}=68.93±0.03 °C) and zinc (T_{fus}=419.53 °C), and verified with naphthalene (T_{fus}=80.20±0.04 °C), benzoic acid (T_{fus}=122.35±0.02 °C), and indium (T_{fus}=156.60 °C). For heat calibration the enthalpy of fusion of indium was used ($\Delta_{fus}H$=3286±13 J mol^{-1}).[24]

The quantum chemical calculations were performed with the Gaussian 03 suit of programs[25] at the DFT level of theory, using the 6-311++G(d,p) basis set.[26,27] The three-parameter hybrid density functional abbreviated as B3LYP, which includes Becke's gradient exchange correction[28] and the Lee, Yang and Parr,[29] and Vosko, Wilk and Nusair correlation functionals[30] was selected for the calculations. Structures were optimized using the Geometry Direct Inversion of the Invariant Subspace (GDIIS) method,[31,32] with the transition state structures for conformational interconversion located using the Synchronous Transit-Guided Quasi-Newton (STQN) approach.[33] The 2D potential energy surface maps were built by varying the N_3–C_4–N_{10}–C_{11} and C_4–N_{10}–C_{11}–O_{14} dihedral angles from 0 to 360° in increments of 5° and optimizing all other structural parameters at the selected level of theory.

Vibrational frequencies were calculated at the same level of theory and scaled down by a single factor (0.978) to correct them mainly for the effects of basis set limitations, neglected part of electron correlation and anharmonicity effects, and used to assist the analysis of the experimental spectra. Normal coordinate analysis of allantoin was undertaken in the internal coordinates space as described by Schachtschneider,[34] using the program BALGA and the optimized geometries and harmonic force constants resulting from the DFT(B3LYP)/6-311++G(d,p) calculations.

3. Results and discussion

3.1. Conformational analysis

Allantoin has a chiral center, the two enantiomers being conformationally and spectroscopically equivalent. In this study we will then consider only one of the enantiomers (S form).

According to the 2D potential energy map shown in Figure 2, at least four conformers differing in the N_3–C_4–N_{10}–C_{11} and C_4–N_{10}–C_{11}–O_{14} dihedral angles were expected for the molecule. This number could, eventually, increase if the heterocyclic ring deviated from planarity and the imide and amide groups were pyramidalized. Hence, a detailed search for conformers was undertaken by varying the initial geometries of the imide and amide groups and also including structures with a non-planar heterocyclic ring in the set of structures submitted to full geometry optimization. All these structures corresponded to geometries located in the vicinity of the four general minima found in the preliminary relaxed scan performed to build the 2D potential energy map provided in Figure 2.

The final number of located different energy minima was 6 (Fig. 3). Nevertheless, as discussed in detail below, these six minima correspond to only four conformational states, each one associated with one of the four low potential energy valleys represented in Figure 2.
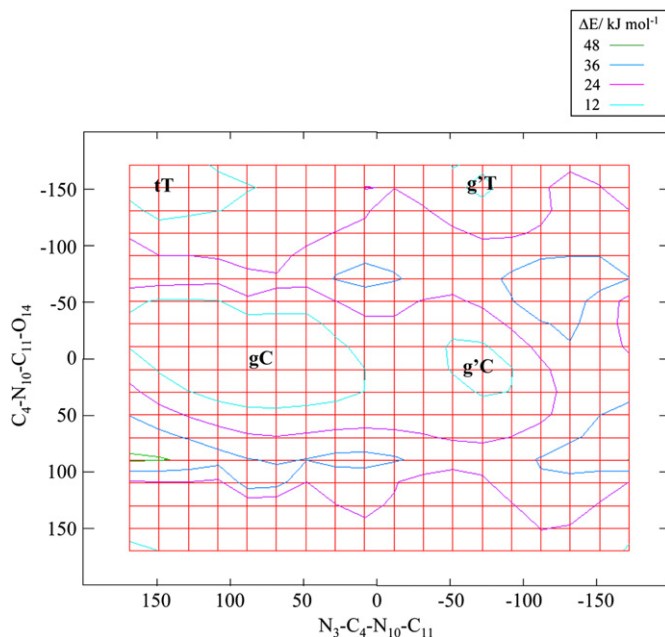
Figure 2. Potential energy map for allantoin. The map resulted from a relaxed potential energy scan where the N_3–C_4–N_{10}–C_{11} and C_4–N_{10}–C_{11}–O_{14} dihedral angles were varied from 0 to 360° in increments of 5° and all other structural parameters optimized at the DFT/B3LYP/6-311++G(d,p) level of theory. The plot shows four valleys, which were then fully explored for identification of the conformers of the molecule (see text for details).

In the 60/0° valley (N_3–C_4–N_{10}–C_{11}/C_4–N_{10}–C_{11}–O_{14}), two minima were located (I and I′), which differ mainly in the geometry of the exocyclic NH_2 and NH groups (see Fig. 3) and are separated from each other by a transition state whose energy is less than 0.01 kJ mol⁻¹ above that of the highest energy I′ minimum. So, in practical terms, I and I′ can be seen as a single conformer: the highest energy I′ form can be considered as a vibrationally excited state of I, because the barrier separating this form from I is below its zero point energy level. According to the values of its N_3–C_4–N_{10}–C_{11} and C_4–N_{10}–C_{11}–O_{14} dihedral angles, we named minimum I as conformer **gC**. This is the lowest energy minimum of allantoin.

Single minima were located both in the 180/180° and −60/180° valleys, corresponding to the **tT** and **g′T** conformers, respectively (Fig. 3). These forms are higher in energy than **gC** by ca. 11 and 18 kJ mol⁻¹.

Finally, in the −60/0° valley, like in the 60/0° valley, two minima (III and III′) were found with different orientations of the amide group (Fig. 3), but also in this case the highest energy minimum (III′) is better described as a vibrationally excited state of the lowest energy minimum (III). Minimum III corresponds to the **g′C** conformer of allantoin, which has a relative energy of ca. 14 kJ mol⁻¹.

Table 1 summarizes the energetic data resulting from the calculations, including the barriers for conformational isomerization between the different forms. The calculated optimized geometries for the six minima found on the potential energy surface of allantoin are provided as Supplementary data (Table S1).

It is easy to conclude that the relative stability of the conformers results mainly from the different H-bond like interactions they exhibit. The most stable **gC** conformer possesses two considerably strong N–H···O═ bonds (N_3–H_9···O_{14}═ and N_{10}–H_{13}···O_6═), which justify its comparatively low energy. The second most stable conformer, **tT**, has also two H-bond interactions (N_{12}–H_{15}···O_6═ and N_{10}–H_{13}···N_3), which, however, are weaker than those in the conformational ground state. In turn, the third and fourth conformers in order of energy (**g′C** and **g′T**, respectively) do not exhibit any H-bond or have only one weak H-bond like interaction (N_{12}–H_{15}···N_3).
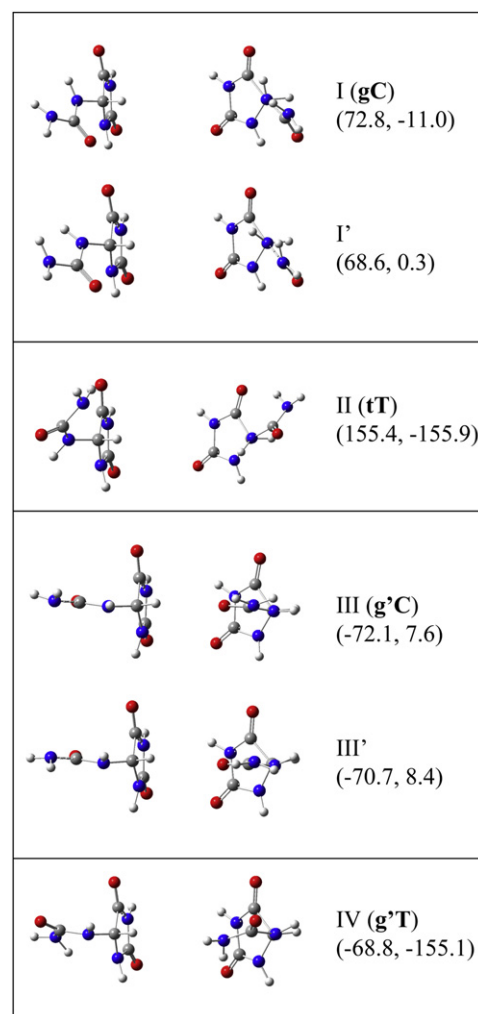

Figure 3. DFT/B3LYP/6-311++G(d,p) optimized geometries (two perspectives) of the six minima found on the potential energy surface of allantoin. In parentheses the values of the N_3–C_4–N_{10}–C_{11} and C_4–N_{10}–C_{11}–O_{14} dihedral angles (in degrees).

Table 1
DFT/B3LYP/6-311++G(d,p) calculated energies for the minima and transition state (TS) structures on the potential energy surface of allantoin and dipole moments for the relevant minima

Minima/TS	Conformer	Energy/Hartree	ΔE/kJ mol⁻¹	μ/Debye
I	**gC**	−600.9735194	0.00	3.57
I′		−600.9727559	2.00	
II	**tT**	−600.9693672	10.90	2.68
III	**g′C**	−600.9683094	13.68	6.06
III′		−600.9680536	14.35	
IV	**g′T**	−600.9667005	17.90	3.35
TS(I′→I)		−600.9727542	0.0045	
TS(III′→III)		−600.9678236	0.60	
TS(II→I)		−600.9570749	32.27	
TS(III→I)		−600.9626044	14.98	
TS(IV→II)		−600.9597735	18.19	
TS(IV→III)		−600.9532547	35.30	

3.2. Energy barriers for conformational interconversion

As already mentioned, the barriers between the two **gC** minima and between the two **g′C** minima, measured from the bottom of the potential wells of the highest energy member of each pair, are very low (below 1 kJ mol⁻¹; see Table 1). Hence, as referred to above, in practical terms each pair of minima corresponds to a single
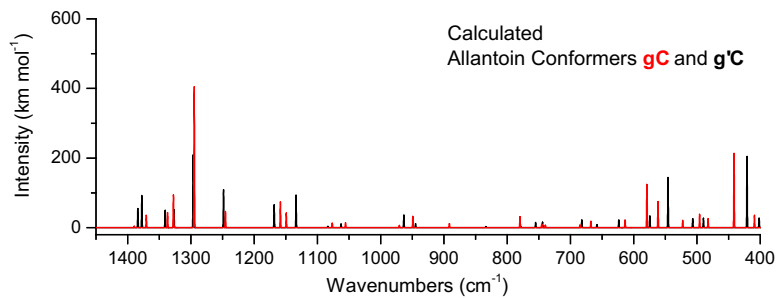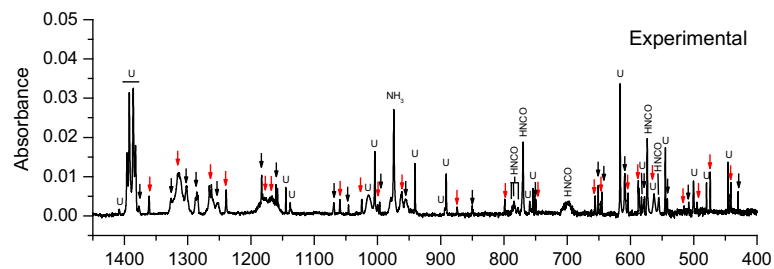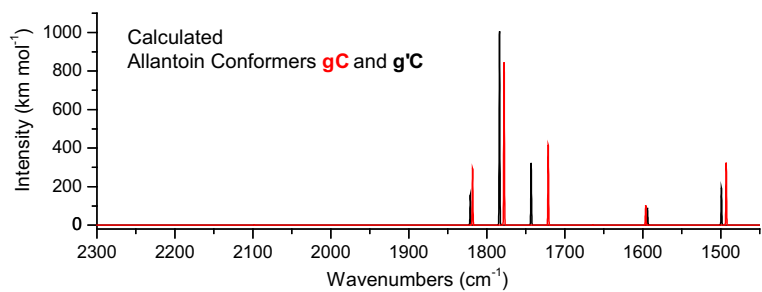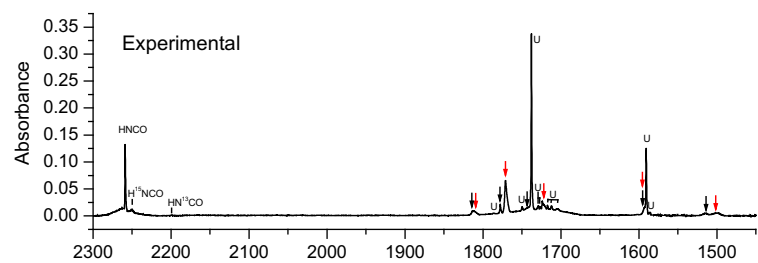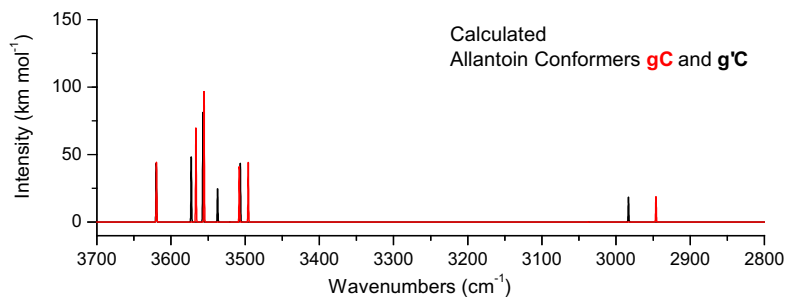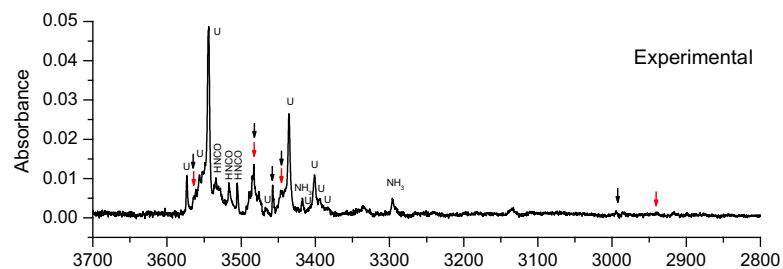
conformer. The barriers between the two C and between the two T conformers are 14.98 (**g′C→gC**) and 18.19 kJ mol^{-1} (**g′T→tT**), respectively, whereas that between the two lowest energy forms, **tT** and **gC**, is as large as 32.27 kJ mol^{-1}. In relation with the matrix isolation experiments described in this paper, all these barriers may be considered high enough to preclude any isomerization to take place both during deposition and upon annealing of the matrices (conformational cooling[35–37]). This fact opened some perspectives regarding the possible observation of more than one conformer of allantoin in the matrix isolation infrared spectra if the compound could partially survive to the deposition procedure. On the other hand, using the Boltzmann statistics and the calculated relative energies of the conformers, their equilibrium populations could be estimated to be 98.3/1.2/0.4/0.1% (**gC/tT/g′C/g′T**) at room temperature and 90.2/5.9/2.9/1.0% at ca. 200 °C (approximate maximum temperature applied to the crystalline sample of allantoin to prepare the matrices). Hence, the possibility of experimental observation of both **tT** and **g′T** forms looked in fact very improbable, while that of observing **g′C** form could not be excluded a priori, since in the crystal allantoin molecules exist exclusively in this conformation.[21] As it will be shown in detail below, in agreement with these expectations, we could found experimental evidence of both **gC** and **g′C** conformers of allantoin in the matrix isolation IR spectra, as minor species, together with its decomposition products.

3.3. Allantoin isolated in argon matrix and identification of the products of its thermal decomposition

The DSC experiments carried out on the compound placed in a hermetically sealed pan showed that allantoin starts to decompose simultaneously with the melting, at about 230 °C. These results show the thermal lability of the compound. However, under low pressure conditions, as those used in the matrix isolation experiments ($P=10^{-6}$ mbar), it appeared possible that the compound could survive to decomposition, at least partially, and, as already mentioned, this was confirmed in practice.

Figure 4 shows the matrix isolation IR spectra obtained from heating allantoin and fast depositing the produced vapors onto the cold (10 K) substrate of the cryostat. The spectrum reveals very clearly the presence of urea and isocyanic acid as main products of thermal decomposition of allantoin. Besides these two substances, the matrix also indicates the presence of NH$_3$ and a minor fraction of non-decomposed allantoin. Comparison of the experimental data with the calculated spectra for the different conformers of allantoin showed that in the matrix allantoin exists in two different conformational states: the conformer existing in the crystalline state (**g′C**) and the most stable one in gas phase (**gC**). Analysis of the sample holder after the experiment revealed also the presence of a residue of carbon. Figure 5 shows the proposed set of processes resulting in the observed chemical species: (i) ring fragmentation of allantoin, yielding isocyanic acid and (ii) cleavage of the C$_4$–N$_{10}$ bond accompanied by migration of H$_{17}$ resulting in formation of urea; carbon is formed as residue of (i) and (ii). The formed urea can then decompose partially to isocyanic acid and NH$_3$. Simultaneously, a minor amount of allantoin molecules that survived to heating land on the cold surface of the cryostat in the conformation existing in the crystalline sample (**g′C**) or, after conformational isomerization in the gas phase along deposition, as the gas phase most stable conformer **gC**.
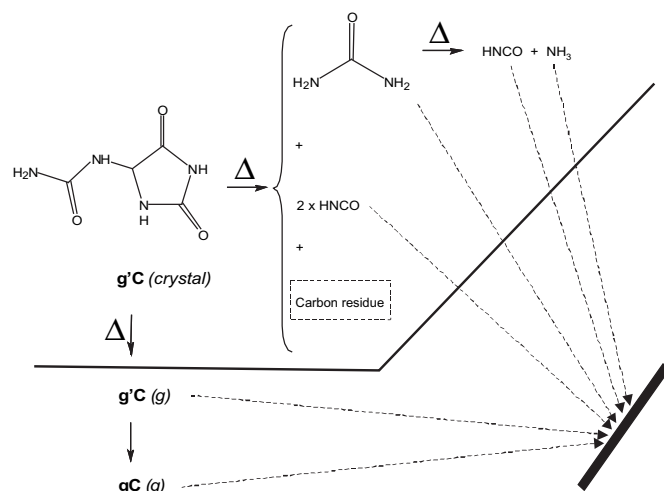

Figure 5. Schematic representation of the observed thermal decomposition processes and conformational isomerization of allantoin.

The infrared spectrum of matrix isolated urea is well known. A comprehensive study of urea and several of its isotopomers in argon matrix was reported by Dobrowolski et al.[38] A one-to-one correspondence between the bands reported by Dobrowolski et al.[38] and those assigned to urea in the spectrum resulting from allantoin decomposition could be established (Table 2), testifying unequivocally that urea has been produced and could be efficiently isolated in the low temperature matrix. Decomposition of allantoin into urea was already reported on heating the compound in the presence of water,[39] in a process, which also gives rise to allanturic acid (C$_3$H$_4$O$_3$N$_2$). The latter molecule, however, was not observed in our experiments, since for its production a water molecule is required, which is unavailable under the present experimental conditions.

The observed NH$_3$ results from decomposition of urea, accompanied by formation of isocyanic acid. This is a well documented process[40,41] that has recently been shown to be the most favorable decomposition pathway for an isolated urea molecule.[41] The presence of NH$_3$ in the studied argon matrix was doubtlessly established by observation of the characteristic band at 974 cm^{-1} due to the umbrella mode,[42–44] and further confirmed by observation of a few additional bands that were previously found[44] to be good indicators of NH$_3$ in argon matrix.

Isocyanic acid results from two different processes: it is produced directly from allantoin and also from decomposition of the previously formed urea, as described above (see also Fig. 5). Isocyanic acid has been studied extensively in low temperature inert matrices and its infrared spectrum in argon matrix is then well known.[16,45–48] As shown in Table 2, the infrared signature of isocyanic acid is easily identifiable in the obtained matrix isolation spectra. Indeed, not just the very characteristic band at 2259 cm^{-1}, assigned to the νNCO asymmetric stretching vibration, could be observed, but all other previously reported IR bands of matrix isolated isocyanic acid, including those reflecting the fact that the HNCO molecule isolated in argon can rotate almost freely along its *a* axis[45,48] and, in the case of the νNCO asymmetric stretching vibration, even those bands originated in minor isotopomers of the compound (HN^{13}CO and H^{15}NCO); see Figure 4 and Table 2.

Figure 4. *Top panel.* Matrix isolation IR spectrum obtained upon heating a sample of allantoin (*RS*-crystal) under vacuum (10^{-6} mbar) and depositing the produced vapor together with argon onto a CsI substrate cooled to 10 K. *Lower panel.* DFT(B3LYP)/6-311++G(d,p) calculated infrared spectra for allantoin conformers **gC** (red) and **g′C** (black). In the experimental spectrum the bands due to the allantoin conformers are indicated by arrows with the same color of their corresponding calculated spectra represented in the lower panel; U=urea. The spectrum was subjected to base line correction and subtraction of bands due to atmospheric H$_2$O and CO$_2$ as well as those resulting from the presence in the matrix of trace amounts of these two substances. The wavenumbers in the calculated spectra correspond to scaled values (scale factor: 0.978). The bands are simulated by Gaussian functions centered at the absorption wavenumber and area equal to the calculated intensity. Three different spectral regions are shown: 3700–2800 cm^{-1}, 2300–1450 cm^{-1}, and 1450–400 cm^{-1}.

Table 2
Infrared spectrum obtained upon deposition of a sample of allantoin as described in the Experimental section

Experimental[a]			Calculated (allantoin)[b]		Assignment	
This work	Others	Ref.	gC	g′C	Species[c]	Mode[d]
3574	3573.6	38			Urea	νNH_2 as.
3563				3620		νNH_2 as.
3560			3619			νNH_2 as.
3556	3556.4	38			Urea	
3552	3552.3	38				νNH_2 as.
3550	3550.4	38				
3545	3544.6	38			Urea	νNH_2 as.
3544	3543.9	38				
3536	e	45			HNCO	
3534	e	45				$\nu NH\ 1\leftarrow0$
3529	e	45				
3516	3516.8	45			HNCO	$\nu NH\ 0\leftarrow0$
3505	3505.7	45				
3493, 3489				3572		νNH (ring)
3485			3566			νNH (ring)
3483, 3481			3555			νNH (ring)
3476, 3473				3557		νNH (ring)
3463	3463.0	38			Urea	νNH_2 s.
3457				3537		νNH (imide)
			3507			νNH_2 sym.
3441				3506		νNH_2 s.
			3495			νNH (imide)
3440	3439.9	38			Urea	νNH_2 s.
3435	3436.2	38			Urea	νNH_2 s.
3433	3433.1	38				
3417	3417.0	44			NH_3	νNH_3 as.
3409	3411.8	38			Urea	
3401	3402.9	38				
3399	3401.8	38				νNH_2 s.
3395	3399.2	38				
3383	3382.9	38				
3336					?	
3296	3296.8	44			NH_3	νNH_3 s.
3135					?	
2995, 2985				2983		νCH
2941			2945			νCH
2259	2259.0	45			HNCO	νNCO as. $0\leftarrow0$
2250	2250.8	45			$H^{15}NCO$	$\nu^{15}NCO$ as.
2199	2199.0	45			$HN^{13}CO$	$\nu N^{13}CO$ as.
1813				1820		$\nu C=O$ (ring)
1812			1817			$\nu C=O$ (ring)
1786	1785.6	38			Urea	$\nu C=O$
1778				1782		$\nu C=O$ (ring)
1771			1777			$\nu C=O$ (ring)
1750	1752.1	38			Urea	$\nu C=O$
1742				1742		$\nu C=O$ (amide)
1737	1737.9	38			Urea	
	1736.5	38				$\nu C=O$
1729	1728.7	38				
1724, 1722			1721			$\nu C=O$ (amide)
1717	1717.6	38				
1712	1712.0	38			Urea	$\nu C=O$
1704	1704.9	38				
			1595			δNH_2
1592				1593		δNH_2
	1593.1	38			Urea	δNH_2 as.
1591	1590.8	38			Urea	δNH_2 as.
1586	1587.0	38			Urea	δNH_2 s.
1515				1498		δNH (imide)
1500			1492			δNH (imide)
1408	1408.3	38			Urea	
1396	1396.0	38				
1392	1392.3	38				νCN as.
	1391.1	38				
1386	1386.2	38				
1382	1382.7	38				
1377				1377		ν ring
1361			1370			ν ring
1326				1340		γCH
1316			1336			γCH
1314, 1313, 1311			1327			δNH (ring)
1301				1327		δNH (ring)
1287, 1285, 1284				1296		$\nu C_{11}-N_{12}$
1265, 1264, 1262			1294			$\nu C_{11}-N_{12}$

Table 2 (continued)

Experimental[a]			Calculated (allantoin)[b]		Assignment	
This work	Others	Ref.	gC	g′C	Species[c]	Mode[d]
1252				1248		w R-U
1239			1244			w R-U
1182				1168		ν ring
1178			1158			ν ring
1167			1149			νC$_4$–N$_{10}$
1161, 1158				1133		νC$_4$–N$_{10}$
1145	1145.0	38			Urea	γNH$_2$ s.
1138	1138.2	38				
1068				1083		wNH$_2$
1058			1076			wNH$_2$
1045				1062		ν ring
1024			1055			ν ring
1012	1008.7	38			Urea	γNH$_2$ as.
1004	1004.3	38				
1000			970			νC$_{11}$–N$_{10}$
996				963		umbrella
978, 974	974.3	44			NH$_3$	ν ring
962			949			
955				945		νC$_{11}$–N$_{10}$
940	940.8	38			Urea	νCN s.
893, 891	891.4	38				
874			891			ν ring
850				833		γ R-U
799			780			γC=O (amide)
785	821.6	45			HNCO	δHNC 1←0
783	819.1	45				
778	790.7	45			HNCO	δHNC 1←1
771	771.0	38			Urea	γC=O
770	769.8	45			HNCO	δHNC 0←0
759	759.3	38			Urea	γC=O
754	754.2	38				
751				744		γC=O (ring)
750			740			γC=O (ring)
697	697.0	45			HNCO	γNCO 1←0
656			684			δC=O (amide)
651				682		δ ring
647			667			γC=O (ring)
645				658		γC=O (ring)
	635.9	38			Urea	δC=O
616	616.4	38				
609				623		δ ring
604			613			δ ring
587			579			γNH (ring)
582	582.4	38			Urea	τNH$_2$ as.
578				574		γNH (ring)
574	573.7	45			HNCO	δNCO 0←0
562			561			δ ring
	550.6	38			Urea	τNH$_2$ s.
555	554.5	45			HNCO	δNCO 1←1
545	544.8	38			Urea	τNH$_2$ s.
541				546		γNH (ring)
515			522			γNH (ring)
508				506		γNH$_2$
500	500.5	38			Urea	?
495			496			γNH$_2$
	483.7	38			Urea	δNCN
479	480.0	38				
473			482			γNH (ring)
445	445.1	38			Urea	wNH$_2$ s.
442, 441		441				γNH (imide)
429				421		γNH (imide)

[a] Wavenumbers in cm^{-1}.

[b] Scaled wavenumbers.

[c] Only decomposition products are indicated. Whenever a band is assigned to allantoin itself this entry is left empty and only the general description of the mode is provided.

[d] ν, stretching; δ, bending; w, wagging; γ, rocking; τ, torsion; as., anti-symmetric; s., symmetric. For allantoin, only a general description of the modes is provided. For a detailed vibrational analysis and full mode characterization, see Tables S3 and S4—Supplementary data.

[e] The wavenumbers for these bands were not reported in Ref. 45, though the observed triplet of bands is discussed in the text (from Fig. 7 of Ref. 45 it can be seen that the triplet of bands stays roughly between 3540 and 3525 cm^{-1}, as observed in the present study).

Identification of allantoin as a minor species in the matrix isolation spectra was made promptly by analysis of the carbonyl stretching region (1850–1700 cm^{-1}; see Fig. 4b), since the bands observed above 1750 cm^{-1} could not be ascribed to any of the expected products of decomposition of allantoin whereas they fit nicely the calculated spectra for allantoin in this spectral region. In particular, comparison of the experimental spectrum with the DFT calculated spectra for the different minima of allantoin revealed that both conformers **gC** and **g′C** contribute to the experimental spectrum. In the carbonyl stretching region, the three expected IR

bands due conformer **gC** were predicted at 1817, 1777, and 1720 cm^{-1} and observed at 1812, 1771, and 1724 cm^{-1}, respectively, while those due to conformer **g′C** were calculated to occur at 1820, 1782, and 1742 cm^{-1} and observed at 1813, 1778, and 1742 cm^{-1}. As shown in Figure 4 and Table 2, besides the bands observed in the carbonyl stretching region, many other bands due to allantoin **gC** and **g′C** conformers could be identified in the experimental matrix isolation spectrum. While some of the proposed assignments must be considered as tentative, the general fitting between the predicted infrared spectra for these conformers (see Tables S2–S4 in the Supplementary data for full theoretical IR data) and their experimentally observed vibrational signature is very good and allows for the unequivocal identification of these species. On the other hand, in consonance with our expectations based on the theoretical conformational analysis no evidence of conformers **tT** and **g′T** was found experimentally. The comparison of the predicted spectra for all four conformers of allantoin can be made based on Table S5 (Supplementary data). A selected spectral region is shown in Figure 6, where the experimental spectrum is compared with
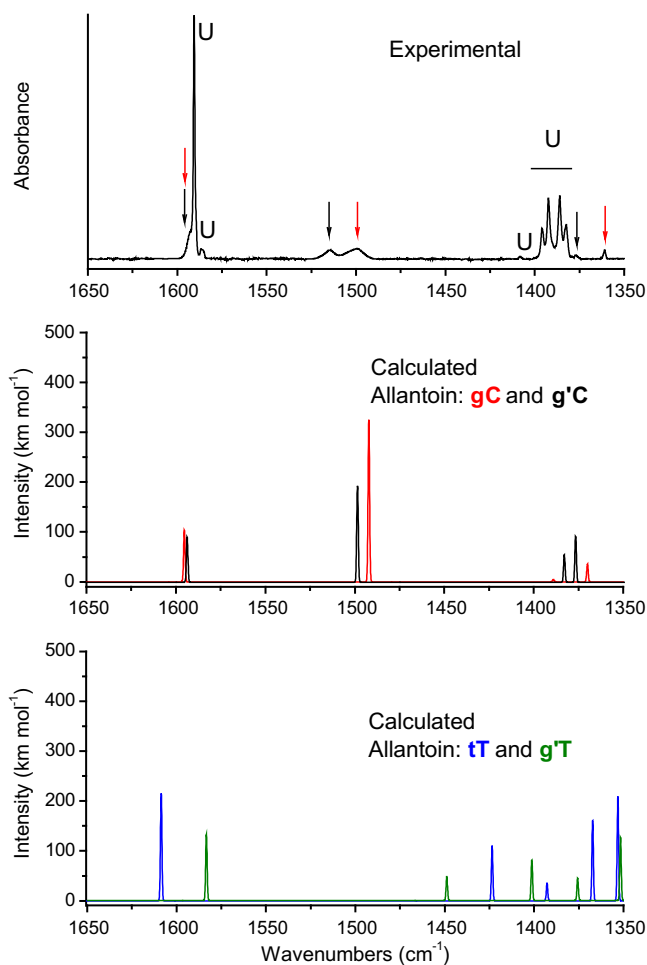
those of the different conformers. From this figure it is clear that only conformers **gC** and **g′C** contribute to the spectrum of the obtained matrix, whereas **tT** and **g′T** are absent, e.g., the intense bands of the **tT** conformer predicted to occur at 1608, 1423, and 1353 cm^{-1} have no experimental counterpart, as well as those predicted for **g′T** at 1583, 1449, 1401, and 1352 cm^{-1}. Other intense bands calculated for these two conformers expected to appear in sparsely populated spectral regions that could not be observed in the experimental spectrum, thus further supporting our conclusion, are those predicted at 1119 cm^{-1} (**tT**) and 1140 and 1101 cm^{-1} (**g′T**) (see Fig. 4 and Table S5).

3.4. Infrared spectrum of crystalline allantoin at room temperature

The infrared spectrum of crystalline allantoin had never been studied in detail before. This spectrum is shown in Figure 7. Comparison of this spectrum with that predicted for the relevant isolated monomer (**g′C**) as well as the spectrum of urea[49] allowed to undertake its assignment, as shown in Table 3.

When compared with the spectrum of the isolated monomer, the spectrum of the crystal exhibits the expected[50–53] pronounced
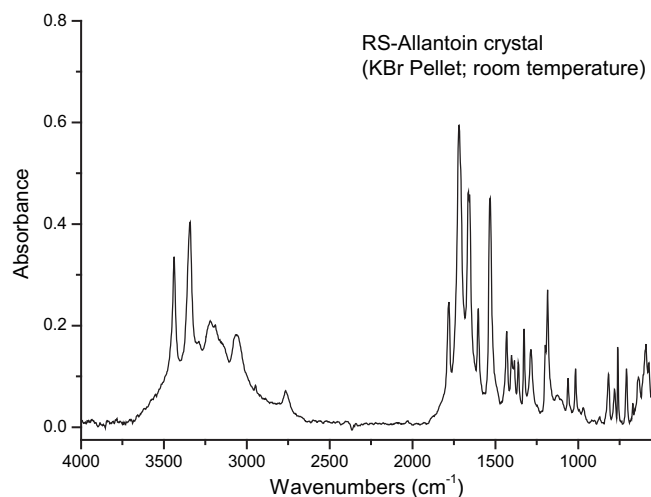

Figure 6. *Top panel*. 1650–1350 cm^{-1} region of the matrix isolation IR spectrum obtained upon heating a sample of allantoin (*RS*-crystal) under vacuum (10^{-6} mbar) and depositing the produced vapor together with argon onto a CsI substrate cooled to 10 K. *Mid and lower panels*. DFT(B3LYP)/6-311++G(d,p) calculated infrared spectra for allantoin conformers **gC** (red), **g′C** (black), **tT** (blue), and **g′T** (green). In the experimental spectrum the bands due to the allantoin conformers are indicated by arrows with the same color of their corresponding calculated spectra represented in the lower panels; U=urea. The spectrum was subjected to base line correction and subtraction of bands due to atmospheric H$_2$O as well as those resulting from the presence in the matrix of trace amounts of this substance. The wavenumbers in the calculated spectra correspond to scaled values (scale factor: 0.978), The bands are simulated by Gaussian functions centered at the absorption wavenumber and area equal to the calculated intensity.

Figure 7. Room temperature infrared spectrum of *RS*-allantoin crystal in KBr pellet.

Table 3
Infrared observed wavenumbers (cm^{-1}) and assignment for crystalline allantoin (*RS*-crystal) in KBr pellet at room temperature[a]

Wavenumber	Assignment	Wavenumber	Assignment
3438	νNH$_2$ as.	1326	νC$_{11}$–N$_{12}$
3343	νNH (ring)	1285	w R-U
3289		1198	ν ring
3221		1185	νC$_4$–N$_{10}$
3191		1125, 1101	wNH$_2$
3148	νNH (imide)	1061	ν ring
3066	νNH$_2$ s.	1016	ν ring
2948	νCH	969	γ R-U
2766	1719+1061	870	νC$_{11}$–N$_{10}$
1781	νC=O (ring)	817	ν ring
1719	νC=O (ring)	780	γC=O (amide)
1663, 1666	νC=O (amide)	761	γC=O (ring)
1603	δNH$_2$	708	δ ring
1532	δNH (imide)	670	γC=O (ring)
1432	δNH (ring)	636	δ ring
1402	ν ring	591	γNH (ring)
1385	γCH	574	γNH (ring)
1361	δNH (ring)	557	γNH$_2$

[a] ν, stretching; δ, bending; w, wagging; γ, rocking; as., anti-symmetric; s., symmetric; R-U means movements of the ring (R) in relation to the ureidyl moiety (U). See Figure 1 for atom numbering.

down shifts of the stretching bands associated with the groups taking part in intermolecular H-bonding (e.g., νNH_2, νNH, and $\nu C=O$ modes; see Tables 2 and 3) and up shifts of the corresponding bending modes (δNH, γNH, γNH_2, $\gamma C=O$).

Most of the bands associated with the ureidyl fragment in crystalline allantoin were found at very similar positions when compared with the analogous vibrations in urea,[49] i.e., νNH_2 between 3450 and 3050 cm^{-1} (as a broad complex band), $\nu C=O$ at 1666/1663 cm^{-1} (1686 cm^{-1} in urea), δNH_2 at 1603 (1631 and 1606 cm^{-1} in urea), wNH_2 at 1125/1101 cm^{-1} (urea: 1153 cm^{-1}) and $\gamma C=O$ at 780 cm^{-1} (urea: 789 cm^{-1}), which points to a similar environment of the ureidyl fragment in allantoin crystal compared to crystalline urea. On the other hand, the νCN bands are observed in allantoin at somewhat lower wavenumbers (1326 and 870 cm^{-1}) than in urea (1468 and 1005 cm^{-1} [49]), as it could be expected taking into account the more extensive coupling with other skeletal vibrations in the studied compound.

4. Conclusions

The detailed investigation of the DFT(B3LYP)/6-311++G(d,p) potential energy surface of allantoin revealed the existence of four conformers (**gC**, **tT**, **g′C**, and **g′T**). The **gC** form was found to be the most stable conformer in gas phase, contrarily to what was observed in the crystalline state (*RS*-allantoin[21]), where the **g′C** conformer was found to be the constituting monomeric unit. This fact stresses the importance of intermolecular H-bonding in determining the structure of the crystal.

Upon sublimation under vacuum (10^{-6} mbar), the compound was found to undergo extensive decomposition to urea, isocyanic acid, NH_3, and carbon. The identification of the decomposition products was successfully made by using matrix isolation infrared spectroscopy, with the spectroscopic fingerprint of all the reaction products clearly depicted in the matrix isolation infrared spectrum. In consonance with the theoretical predictions, in particular the relative energies of the different conformers of allantoin and the energy barriers separating these forms, allantoin molecules surviving thermal decomposition were found to undergo conformational isomerization in the gaseous phase and be present in the cryogenic argon matrix in both the **gC** and **g′C** conformations.

The solid state room temperature infrared spectrum of allantoin was also investigated and fully assigned.

Acknowledgements

Supplementary data

Supplementary data associated with this article can be found in online version, at doi:10.1016/j.tet.2009.09.088.

References and notes

1. Mendel, L. B.; Dankin, H. D. *J. Biol. Chem.* **1910**, 153.
2. Christman, A. A. *J. Biol. Chem.* **1926**, 173.
3. Robinson, W. *J. Parasitol.* **1935**, *21*, 354.
4. Shestopalov, A. V.; Shkurat, T. P.; Mikashinovich, Z. I.; Kryzhanovskaia, I. O.; Bogacheva, M. A.; Lomteva, S. V.; Prokof'ev, V. P.; Gus'kov, E. P. *Izv. Akad. Nauk.: Ser. Biol.* **2006**, *5*, 541.
5. Simoyi, M. F.; Falkenstein, E.; Van Dyke, K.; Blemings, K. P.; Klandorf, H. *Comp. Biochem. Physiol. B: Biochem. Mol. Biol.* **2003**, *135*, 325.
6. Fujihara, S.; Yamaguchi, M. *Phytochemistry* **1978**, *17*, 1239.
7. Young, K. G.; Wentworth, H. P.; Hawkins, W. W. *J. Pharmacol. Exp. Ther.* **1944**, *81*, 1.
8. Fujiwara, S.; Noguchi, T. *Biochem. J.* **1995**, *312*, 315.
9. Thornfeldt, C. *Dermat. Surg.* **2005**, *31*, 873.
10. Disalvo, R. M. *Chem. Manufact. Cosmetics* **2002**, *3*, 29.
11. Eggensperger, H. *Multiaktive Wirkstoffe für Kosmetika* **1995**, 9.
12. Stark, G. R. *Biochemistry* **1965**, *4*, 2363.
13. Stark, G. R. *Biochemistry* **1965**, *4*, 1030.
14. Haley, R. J.; Ward, D. M. *Am. J. Kidney Dis.* **1986**, *8*, 115.
15. E Roxborough, H.; Young, I. S. *Med. Hypotheses* **1995**, *45*, 125.
16. Gómez-Zavaglia, A.; Reva, I. D.; Frija, L.; Cristiano, M. L.; Fausto, R. *J. Photochem. Photobiol. A: Chem.* **2006**, *179*, 243.
17. Caussé, E.; Pradelles, A.; Dirat, B.; Negre-Salvayre, A.; Salvayre, R.; Couderc, F. *Electrophoresis* **2007**, *28*, 381.
18. Jin, P.; Ma, J.; Wu, X.; Zou, D.; Sun, C.; Hu, X. *J. Pharm. Biomed. Anal.* **2009**, *50*, 293.
19. Kim, K. M.; Henderson, G. N.; Frye, R. F.; Galloway, C. D.; Brown, N. J.; Segal, M. S.; Imaram, W.; Johnson, R. J. *J. Chromatogr., B* **2009**, *877*, 65.
20. Lagendijk, J.; Ubbink, J. B.; Vermaak, W. J. *J. Chromatogr. Sci.* **1995**, *33*, 186.
21. Mootz, D. *Acta Crystallogr.* **1965**, *19*, 726.
22. Kahn, K.; Tipton, P. A. *Bioorg. Chem.* **2000**, *27*, 62.
23. Kahn, K. Kinetic and Mechanistic Characterization of the Urate Oxidase reaction, Ph.D. Thesis, University of Missouri, Columbia, USA, 1998.
24. Sabbahm, R.; Wu, A. X.; Chickos, J. S.; Leitão, M. L. P.; Roux, N. V.; Torres, L. A. *Thermochim. Acta* **1995**, *331*, 93.
25. Frisch, M. J.; Trucks, G. W.; Schlegel, H. B.; Scuseria, G. E.; Robb, M. A.; Cheeseman, J. R.; Montgomery, J. A., Jr.; Vreven, T.; Kudin, K. N.; Burant, J. C.; Millam, J. M.; Iyengar, S. S.; Tomasi, J.; Barone, V.; Mennucci, B.; Cossi, M.; Scalmani, G.; Rega, N.; Petersson, G. A.; Nakatsuji, H.; Hada, M.; Ehara, M.; Toyota, K.; Fukuda, R.; Hasegawa, J.; Ishida, M.; Nakajima, T.; Honda, Y.; Kitao, O.; Nakai, H.; Klene, M.; Li, X.; Knox, J. E.; Hratchian, H. P.; Cross, J. B.; Adamo, C.; Jaramillo, J.; Gomperts, R.; Stratmann, R. E.; Yazyev, O.; Austin, A. J.; Cammi, R.; Pomelli, C.; Ochterski, J. W.; Ayala, P. Y.; Morokuma, K.; Voth, G. A.; Salvador, P.; Dannenberg, J. J.; Zakrzewski, V. G.; Dapprich, S.; Daniels, A. D.; Strain, M. C.; Farkas, O.; Malick, D. K.; Rabuck, A. D.; Raghavachari, K.; Foresman, J. B.; Ortiz, J. V.; Cui, Q.; Baboul, A. G.; Clifford, S.; Cioslowski, J.; Stefanov, B. B.; Liu, G.; Liashenko, A.; Piskorz, P.; Komaromi, I.; Martin, R. L.; Fox, D. J.; Keith, T.; Al-Laham, M. A.; Peng, C. Y.; Nanayakkara, A.; Challacombe, M.; Gill, P. M. W.; Johnson, B.; Chen, W.; Wong, M. W.; González, C.; Pople, J. A. *GAUSSIAN 03 Revision B. 04*; Gaussian: Pittsburgh, PA, 2003.
26. McLean, A. D.; Chandler, G. S. *J. Chem. Phys.* **1980**, *72*, 5639.
27. Krishnan, R.; Binkley, J. S.; Seeger, R.; Pople, J. A. *J. Chem. Phys.* **1980**, *72*, 650.
28. Becke, A. D. *Phys. Rev. A* **1988**, *38*, 3098.
29. Lee, C.; Yang, W.; Parr, R. G. *Phys. Rev. B* **1988**, *37*, 785.
30. Vosko, S. H.; Wilk, L.; Nusair, M. *Can. J. Phys.* **1980**, *58*, 1200.
31. Frisch, M. J.; Head-Gordon, M.; Pople, J. A. *Chem. Phys. Lett.* **1990**, *166*, 281.
[32. Csaszar, P.; Pulay, P. *J. Mol. Struct.* **1984**, *114*, 31.
33. Peng, C.; Schlegel, H. *Isr. J. Chem.* **1994**, *33*, 449.
34. Schachtschneider, J. H.; Mortimer, F. S. *Vibrational Analysis of Polyatomic Molecules. VI FORTRAN IV Programs for Solving the Vibrational Secular Equation and for the Least-Squares Refinement of Force Constants, Project No. 31450. Structural Interpretation of Spectra*; Shell Development: Houston, TX, 1965.
35. Reva, I. D.; Stepanian, S. G.; Adamowicz, L.; Fausto, R. *Chem. Phys. Lett.* **2003**, *374*, 631.
36. Lopes Jesus, A. J.; Rosado, M. T. S.; Reva, I.; Fausto, R.; Eusébio, M. E. S.; Redinha, J. S. *J. Phys. Chem. A* **2008**, *112*, 4669.
37. Rosado, M. T. S.; Lopes Jesus, A. J.; Reva, I. D.; Fausto, R.; Redinha, J. S. *J. Phys. Chem. A* **2009**, *113*, 7499.
38. Dobrowolski, J. C.; Kolos, R.; Sadlej, J.; Mazurek, A. P. *Vib. Spectrosc.* **2002**, *29*, 261.
39. Ware, E. *Chem. Rev.* **1950**, *46*, 403.
40. Schaber, P. M.; Colson, J.; Higgins, S.; Thielen, D.; Anspach, B.; Brauer, J. *Thermochim. Acta* **2004**, *424*, 131.
41. Tokmakov, I. V.; Alavi, S.; Thompson, D. L. *J. Phys. Chem. A* **2006**, *110*, 2759.
42. Bohn, R. B.; Andrews, L. *J. Phys. Chem.* **1989**, *93*, 3974.
43. Bossa, J.; Duvernay, F.; Theulé, P.; Borget, F.; Chiavassa, T. *Chem. Phys.* **2008**, *354*, 211.
44. Lundell, J.; Krajewska, M.; Räsänen, M. *J. Phys. Chem. A* **1998**, *102*, 6643.
45. Teles, J. H.; Maier, G.; Hess, B. A., Jr.; Schaad, L. J.; Winnewesser, M.; Winnewisser, B. P. *Chem. Ber.* **1989**, *122*, 753.
46. Coffey, M. J.; Berghout, H. L.; Woods, E., III; Crim, F. F. *J. Chem. Phys.* **1999**, *110*, 10850.
47. McLean, A. D.; Loew, G. H.; Berkowitz, D. S. *J. Mol. Spectrosc.* **1977**, *64*, 184.
48. Cugley, P. A.; Pullin, A. D. E. *Chem. Phys. Lett.* **1973**, *19*, 203.
49. Stewart, J. E. *J. Chem. Phys.* **1957**, *26*, 248.
50. Rozenberg, M.; Shoham, G.; Reva, I. D.; Fausto, R. *Spectrochim. Acta A* **2004**, *60*, 2319.
51. Rozenberg, M.; Shoham, G.; Reva, I. D.; Fausto, R. *Spectrochim. Acta A* **2004**, *60*, 463.
52. Rozenberg, M.; Shoham, G.; Reva, I. D.; Fausto, R. *Spectrochim. Acta A* **2003**, *59*, 3253.
53. Rozenberg, M.; Shoham, G.; Reva, I. D.; Fausto, R. *Phys. Chem. Chem. Phys.* **2005**, *7*, 2376.